

Wind Modulation of Small-scale Plumes From Yin-Yang Bay

CHUN-TE LIN¹, SHENN-YU CHAO² and KUANG-LUNG FAN¹

(Manuscript received 19 January 1995, in final form 30 October 1995)

ABSTRACT

The unsteady behavior of small-scale plumes emanating from Yin-Yang Bay northeast of Taiwan is dominated by winds, tides and the river (the Lien-Tong Stream) forcing. The three-way interaction is examined here using a three-dimensional primitive-equation model, complementing the earlier tide-plume interaction model for Yin-Yang Bay (Lin *et al.*, 1994). Unlike large-scale plumes, whose wind-induced dispersal primarily follows Ekman drifts, small-scale plumes are dispersed by winds in primarily the windward direction. One exception is that a landward wind compresses plume water shoreward and subjects its eventual dispersal to tidal advection and density forcing. Among winds from all directions, seaward winds are found to be the most effective in dispersing plume water afar. It is argued that wind-induced coastal sea level set-up or set-down always acts to offset Ekman drifts and keeps the current windward. This explains why the wind modulation of small-scale plumes is so different from that of large-scale plumes.

(Key words: Wind modulation, Three-way interaction, Windward direction)

1. INTRODUCTION

In a coupled estuary-shelf environment, the variability of a river-forced plume is primarily driven by winds, tides and the earth's rotation. These three effects can be better quantified by three non-dimensional numbers. The importance of the earth's rotation can be measured by a Kelvin number (K), defined as the ratio of the outlet channel width to the internal Rossby deformation radius. For $K \geq 1$, an anticyclonic bulge is formed near the mouth of the embayment. On the other extreme, for $K \ll 1$, the near-field plume dispersal is seaward, and the anticyclonic turning occurs in the far field. Tidal effects can be measured by a tidal excursion number, P , defined as the ratio of the width of the outlet channel to the tidal excursion length. For $P \gg 1$, the subtidal plume behavior is essentially modulated by the tidal residual eddies induced by the nonlinear transfer of vorticity from oscillating tidal currents to the mean flow. As P decreases to one or less, the tidal effect becomes

¹ Institute of Oceanography, National Taiwan University, Taipei, Taiwan, R.O.C.

² Horn Point Environmental Laboratory, University of Maryland, Cambridge, Maryland, U.S.A.



increasingly advective, and the plume is expected to oscillate with the tidal currents. With winds, a Froude number, F , can be defined as the ratio of the characteristic wind-driven surface current speed to the plume-induced internal wave phase velocity. The plume system is primarily wind-driven if $F \gg 1$, and density-driven if $F \ll 1$; a strong interaction between the two responses is expected if it is in the order of unity.

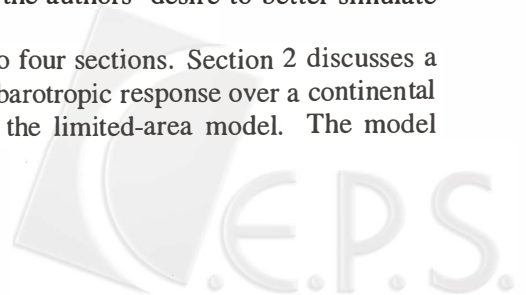
From observation, the Chesapeake Bay plume (Boicourt *et al.*, 1987) off the east coast of the United States is characterized by large K and P . The wind-induced Froude number (F) fluctuates with the winds. The Niagara River plume (Masse and Murthy, 1990) is characterized by $K \geq 1$ and $P \gg 1$. Smaller scale plumes from the Connecticut River (Garvine, 1974) and Mobile Bay, Alabama (Stumpf *et al.*, 1993) have K and P generally of order one. At an even smaller scale, the plume emanating from Yin-Yang Bay off the northeast coast of Taiwan (Lin *et al.*, 1994) is characterized by $K \ll 1$ and $P \ll 1$.

Modeling studies of plumes also scatter about the three-dimensional K - P - F space. Chao and Boicourt (1986) and Chao (1988a) examined the earth's rotational effect on large scale plumes, such as the Chesapeake Bay plume with $K \gg 1$, $F = 0$ and $P \rightarrow \infty$. Wind-plume interaction with $K \gg 1$, $F \sim O(1)$ and $P \rightarrow \infty$ was then examined (Chao, 1988b). Tide-plume interaction was lastly investigated also in the context of large-scale plumes with $K \gg 1$, $F = 0$ and $P \gg 1$ (Chao, 1990). For small-scale plumes with modest tides, $K \sim O(1)$, $P \sim O(1)$, the buoyant outflow vibrates with the tidal currents and shows less Coriolis deflection (O'Donnell, 1990). The numerical simulation of the tide-plume interaction off Yin-Yang Bay (Lin *et al.*, 1994) seems to be of the smallest scale thus far. In the limit of $K \ll 1$ and $P \ll 1$, tidal advection becomes extremely important; the Coriolis deflection is nevertheless unyielding, causing the freshwater dispersal to favor the coast that bounds the plume to the right.

This paper continues the effort of Lin *et al.* (1994) by considering plume dispersal in the presence of both winds and tides in the vicinity of Yin-Yang Bay, extending existing modeling studies to the limits of the smallest scales. In the K - P - F space, this is the limit in which $K \ll 1$, $P \ll 1$ and $F \gg 1$. Although the wind modulation of large-scale plumes was studied earlier (Chao, 1988b), it would be erroneous to generalize its conclusions to a small-scale setting such as Yin-Yang Bay. In the proximity of the shoreline, wind-induced sea level set-up or set-down can be quite large; the consequent pressure gradient force induces responses that differ markedly from those offshore. In this light, the dispersal of small-scale plumes in response to winds should be quite different from that as envisioned by the earlier study (Chao, 1988b). Hence, it seems necessary to rebuild old intuitions concerning the small-scale limit appropriate for Yin-Yang Bay.

In addition to wind forcing, two more improvements are made over the previous tide-plume interaction model of Lin *et al.* (1994). The earlier model basin is enclosed with cyclic boundary conditions in the alongshore direction and a vertical wall at the offshore boundary. The three open ocean boundaries are now given rather realistic open ocean boundary conditions, with the model skills having been extended to simulate unbounded ocean conditions in a limited area. The second improvement is to allow vertical viscosity and diffusivity to depend on the Richardson number according to the formulation of Pacanowski and Philander (1981). The latter measure arises out of the authors' desire to better simulate the wind-driven current in the upper ocean.

The remaining portion of this paper is divided into four sections. Section 2 discusses a set of analytical expressions governing the wind-driven barotropic response over a continental shelf, which can be imposed as boundary forcing on the limited-area model. The model



description is given in Section 3, and the numerical results in Section 4. The discussion and conclusions follow in Section 5.

2. THE WIND-DRIVEN BAROTROPIC RESPONSE OVER THE CONTINENTAL SHELF

Shelf waters off Yin-Yang Bay are distinctively homogeneous even in summer. It is, therefore appropriate, to impose barotropic wind-driven responses over the shelf proper. Analytical solutions based on the models of Csanady (1974, 1984) are established below to facilitate the numerical study.

Consider a semi-infinite ocean bounded by a straight coastline at $y = 0$ and extending to $y \rightarrow \infty$. The water depth is uniform alongshore but deepens in the seaward (y -) direction. Assuming the wind stress (τ_{sx} and τ_{sy} in x and y directions, respectively) is uniform alongshore, it is possible to seek alongshore-uniform solutions which may be taken from the following shallow water equations.

$$\frac{\partial u}{\partial t} - fv = \frac{\tau_{sx} - \tau_{bx}}{\rho h} \quad (1a)$$

$$\frac{\partial v}{\partial t} + fu = -g \frac{\partial \zeta}{\partial y} + \frac{\tau_{sy} - \tau_{by}}{\rho h} \quad (1b)$$

$$\frac{\partial(vh)}{\partial y} = -\frac{\partial \zeta}{\partial t} \quad (1c)$$

where (u, v) are depth-averaged velocities, f is the Coriolis parameter, ζ is the surface elevation about the mean, (τ_{bx}, τ_{by}) are quadratic bottom stresses in (x, y) directions and $h(y)$ is water depth. Spinning up from rest at $t = 0$, velocities and surface elevation are bounded as $y \rightarrow \infty$. At the coastline, normal transport vanishes, resulting in:

$$vh = 0 \quad \text{at} \quad y = 0 \quad (2)$$

With bottom stress ignored for the moment, boundary conditions for u and ζ at $y = 0$ can also be derived as

$$-g \frac{\partial \zeta}{\partial y} = -\frac{F_y}{h}, u = 0 \quad \text{if} \quad F_x = 0 \quad (3)$$

$$-g \frac{\partial \zeta}{\partial y} = fu, \quad \frac{\partial u}{\partial t} = \frac{F_x}{h} \quad \text{if} \quad F_y = 0 \quad (4)$$

For convenience, wind stress is scaled by ρ , making $F_x = \tau_{sx}/\rho$ and $F_y = \tau_{sy}/\rho$.

For a piecewise-linear bottom slope profile which is continuous and reaches a maximum depth of H at some distance offshore, general solutions can be constructed on a piece-by-piece basis. Winds initially drive inviscid coastal currents that are subsequently arrested by bottom friction. Following Csanady (1974), inviscid solutions are sought first, ignoring bottom friction for the moment. It is also useful to nondimensionalize horizontal length scales

by a Rossby radius, $R = \sqrt{gH}/f$. For a uniform alongshore wind ($F_y = 0$), the solution can be written as

$$u = A(y)t \quad (5a)$$

$$v = v(y) \quad (5b)$$

$$\zeta = Z(y)t \quad (5c)$$

For a segment of constant bottom slope stretching out from $y = y_0$ seaward, $h = h_0 + s(y - y_0)$ where $s = dh/dy$. The general solutions are:

$$\frac{A(\lambda)H}{F_x} = \frac{4}{\alpha^2 \lambda} [B_1 K_1(\lambda) + B_2 I_1(\lambda)] \quad (6a)$$

$$\frac{v(\lambda)h(y)f}{F_x} = -1 + \lambda [B_1 K_1(\lambda) + B_2 I_1(\lambda)] \quad (6b)$$

$$\frac{Z(\lambda)\sqrt{gH}}{F_x} = \frac{2}{\alpha} [B_1 K_0(\lambda) + B_2 I_0(\lambda)] \quad (6c)$$

where B_1 and B_2 are constants to be determined later, $K_1(\lambda)$, $I_1(\lambda)$, $K_0(\lambda)$, $I_0(\lambda)$, are modified Bessel functions, and their argument λ , is:

$$\lambda(Y) = \left[\frac{4}{\alpha} (Y - Y_0 + \beta_0) \right]^{\frac{1}{2}} \quad (7)$$

Further, $\alpha = S/R$, where $S = gs/f^2$ is a slope length scale, $Y = y/R$, $Y_0 = y_0/R$ and $\alpha\beta_0 = h_0/H$.

The solution for a segment of the bottom of a constant depth, h_c , is:

$$\frac{A(Y)H}{F_x} = \frac{1}{D_c} [B_3 \exp(\frac{Y}{\sqrt{D_c}}) + B_4 \exp(-\frac{Y}{\sqrt{D_c}})] \quad (8a)$$

$$\frac{v(Y)h_c f}{F_x} = -1 + B_3 \exp(\frac{Y}{\sqrt{D_c}}) + B_4 \exp(-\frac{Y}{\sqrt{D_c}}) \quad (8b)$$

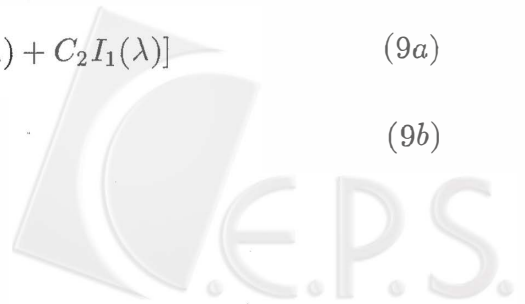
$$\frac{Z(Y)\sqrt{gH}}{F_x} = \frac{1}{\sqrt{D_c}} [B_3 \exp(\frac{Y}{\sqrt{D_c}}) - B_4 \exp(-\frac{Y}{\sqrt{D_c}})] \quad (8c)$$

where (B_3 , B_4) are constants, $D_c = h_c/H$.

For a uniform cross-shelf wind ($F_x = 0$) over a segment of linear bottom slope, solutions are:

$$\frac{u(\lambda)h(y)f}{F_y} = 1 + \lambda [C_1 K_1(\lambda) + C_2 I_1(\lambda)] \quad (9a)$$

$$v = 0 \quad (9b)$$



$$\frac{\zeta(\lambda)\sqrt{gH}f}{F_y} = \frac{2}{\alpha}[C_1 K_0(\lambda) - C_2 I_0(\lambda)] \quad (9c)$$

For a constant depth, solutions are:

$$\frac{u(Y)h_c f}{F_y} = 1 + C_3 \exp\left(\frac{Y}{\sqrt{D_c}}\right) + C_4 \exp\left(-\frac{Y}{\sqrt{D_c}}\right) \quad (10a)$$

$$v = 0 \quad (10b)$$

$$\frac{\zeta(Y)\sqrt{gH}f}{F_y} = -\frac{1}{\sqrt{D_c}}[C_3 \exp\left(\frac{Y}{\sqrt{D_c}}\right) - C_4 \exp\left(-\frac{Y}{\sqrt{D_c}}\right)] \quad (10c)$$

Unknown constants, C_1 , C_2 , C_3 and C_4 , are to be determined by boundary and continuity conditions.

For a model shelf approximated by a series of linear bottom slopes and plateaus, solutions can be obtained by connecting piecewise general solutions together. Unknown constants in (6), (8), (9) and (10) can be determined by applying boundary conditions at and $y = 0$ and $y \rightarrow \infty$, and by demanding surface elevation (ζ) and cross-shelf velocity (v) be continuous across every junction.

Figure 1 shows the nondimensional surface elevation (top), alongshore velocity (middle) and cross-shelf velocity (bottom) as functions of the seaward coordinate (y) for both alongshore and cross-shelf winds. Superimposed on the three panels is the characteristic bottom profile off Yin-Yang Bay. For easy adaptation to the numerical calculation, the model bottom slope is assumed to level off at $y > 9$ km. To retain generality, (ζ , u , v) are nondimensionalized, and in the event that ζ and u accelerate linearly in time under alongshore wind, only $\partial\zeta/\partial t$ and $\partial u/\partial t$ are plotted. For an alongshore wind, the nondimensional forms of (ζ , u , v), (AH/F_x , vhf/F_x , $Z\sqrt{gH}/F_x$), are plotted. For a cross-shelf wind, $\zeta\sqrt{gH}f/F_y$ and uhf/F_y are plotted. In the bottom panel of Figure 1, $v = 0$ for the cross-shelf wind and is, therefore, left out.

Those solutions reveal that the sea level set-up or set-down is concentrated mainly in the first kilometer from the shoreline, decaying continuously offshore. For an alongshore wind, the windward coastal jet is also concentrated in the first kilometer and diminishes farther seaward. For a cross-shelf wind, the alongshore current, however small, is in the direction of the Ekman drift and almost a constant if one takes away the scaling factor, $h(y)$. The cross-shelf current generated by an alongshore wind is generally small and in the direction of the Ekman drift, remaining more or less constant in the cross-shore direction. For a cross-shelf wind, no trans-shelf current is generated.

Under alongshore winds, the linear growth of windward coastal jets and sea level elevations cannot continue indefinitely. At $t = t_f = h(y)/\sqrt{C_{da}F_x}$ and beyond, where C_{da} is the dimensionless bottom drag coefficient for the depth-averaged velocities, the coastal jet is completely arrested by bottom friction and reaches the asymptotic speed. The arresting time scale (t_f) is depth-dependent, vanishing at the coast and progressively increasing farther out. This is the essence of Csanady's coastal jet model, which captures the shelf water responses to the lowest order. Following Csanady's (1984) estimate, C_{da} is chosen to be

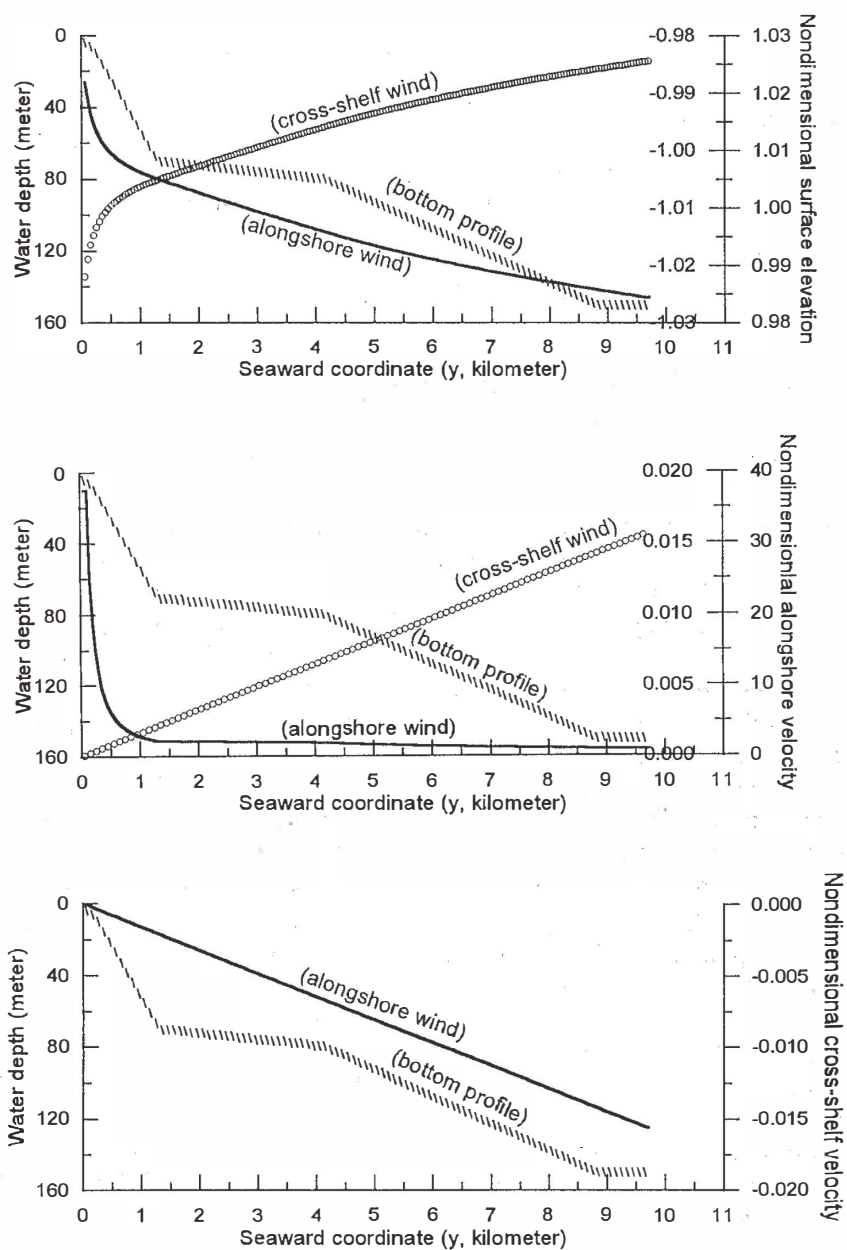


Fig. 1. Nondimensional surface elevation (top), alongshore velocity (middle) and cross-shelf velocity (bottom) as functions of the seaward coordinate (y) for both alongshore and cross-shelf winds. The right vertical axis for the top two panels has two scales, the one on the left for cross-shelf winds, and the one on the right for alongshore winds. The back-slash curve in the three panels is the characteristic bottom profile off Yin-Yang Bay with the depth scales given on left.

one half of the dimensionless bottom drag coefficient C_d which is employed in the three-dimensional numerical model, but the numerical results discussed below are not sensitive to this choice. Further, the change-over from an accelerating jet to an asymptotic jet can be made even smoother by allowing the bottom stress to set in earlier between $t = 0$ and $t = t_f$. However, the added sophistication entails unwieldy mathematics and does not really enhance the model physics to be established below.

3. NUMERICAL MODEL DESCRIPTION

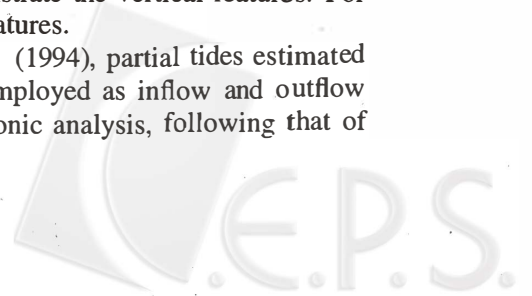
Except for the addition of a free surface (Chao and Paluszkiwicz, 1991), the numerical model employed in this study is a general circulation model (GCM) originally developed by Semtner (1974). The model solves the three-dimensional continuity, momentum and salinity equations under Boussinesq and hydrostatic approximations. Horizontal mixing is achieved by using an eddy viscosity of $5000 \text{ cm}^2 \text{ s}^{-1}$ in momentum and eddy diffusivity of $500 \text{ cm}^2 \text{ s}^{-1}$ in salinity equations. The time-varying vertical viscosity and diffusivity are calculated from the Richardson number according to the formulae of Pacanowski and Philander (1981). The salinity and vertical shear of the horizontal velocity components are resolved with an internal-mode time step of 12 sec, while the sea level elevation and the depth-averaged horizontal velocities are calculated with a much smaller time step of 0.3 sec. The estimation of the vertical mixing coefficient, mode-splitting technique and inflow/outflow conditions have also been applied to the same GCM by Shaw and Chao (1994). Zero salt flux and momentum flux of wind stress forcing is applied to the sea surface. At the bottom, salt flux normal to the boundary vanishes, and a quadratic drag law with a dimensionless drag coefficient is used for bottom friction. According to the bottom boundary layer theory, the bottom drag coefficient is calculated by:

$$C_d = \left[\frac{1}{k} \ln \left(\frac{H + z_b}{z_0} \right) \right]^{-2} \quad (11)$$

where C_d is the bottom drag coefficient, H the water depth, z_b the depth of the grid point nearest to the bottom, k the von Karmen constant and z_0 the local bottom roughness equal to 1 cm here. The actual algorithm sets C_d to the larger of the two values given by (11) and 0.0025. The estimation of the bottom drag coefficient follows essentially that of Blumberg and Mellor (1987). The model basin consists of realistic Yin-Yang Bay geometry and the adjacent shelf as described by Lin *et al.* (1994). The model resolution is 50 m in the horizontal and 2 m in the vertical. The area coverage is 6 km alongshore and 2 km seaward. The number of vertical layers ranges from 2 well inside the embayment to 25 near the offshore open boundary. All solid vertical boundaries are impenetrable, impermeable and no-slip. More quantitative descriptions of the model can be found in Lin *et al.* (1994).

The vertical resolution is finer than most of the nearshore numerical models of this type. However, since the plume coming out of Yin-Yang Bay is generated by a weak source of freshwater discharge, it is mostly confined to the top 2 m of the water column over the shelf. The shallowness makes it somewhat difficult to demonstrate the vertical features. For this reason, the ensuing illustrations are limited to surface features.

Instead of using a tidal generating force as in Lin *et al.* (1994), partial tides estimated from current data off Yin-Yang Bay (Li *et al.*, 1991) are employed as inflow and outflow conditions on all three offshore open boundaries. The harmonic analysis, following that of



Lien (1977), reveals that the observed tidal currents are essentially alongshore and dominated by M_2 tide. For simplicity, only M_2 tide is employed to facilitate the numerical study.

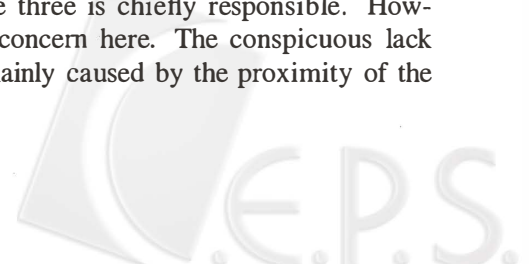
Open boundary conditions are as follows. On the Lien-Tong Stream outlet located at the southwest perimeter of Yin-Yang Bay, salinity is set at 15 psu, while the velocities are required to vanish. On all three open boundaries bounding the limited area over the adjacent shelf, depth-averaged velocities, whether wind-driven or tidally induced or both, are specified. The sea level elevation and velocity deviation from the vertical mean on these three boundaries are extrapolated from the nearest grid points in the interior domain. The salinity values near open boundaries are dictated by advection. If there is an inflow, the salinity outside the domain is given the ambient value (35 psu). These open boundary conditions are in keeping with Shaw and Chao (1994).

The basin is initially filled with motionless sea water of 35 psu salinity. To spin up, tidal forcing is first employed alone for five days to establish equilibrium tides. Thereafter, either river forcing is switched on in concert with tides for three days, or both wind and river are turned on for three days in conjunction with tides. Winds are from the east, west, north or south and have a constant amplitude of 1 dyne/cm^2 . The five experiments (one with tides and plumes, the other four with wind, tides and plumes) form the basis of the present study, each one being 3 days in duration. In addition to these experiments, it is also necessary to conduct wind-only experiments in which winds from the all 4 directions are used to drive the coastal ocean for two days to equilibrium, which also better isolates the role of each forcing.

A few remarks on wind-driven responses are in order. The small size and shallowness of the domain ensures a fast adjustment to equilibrium in response to wind forcing. The time series of the total kinetic energy contained in the basin indicate that this occurs in less than two days. Further, wind forcing cannot be fully accounted for unless it enters the domain from both the sea surface and open boundaries. The former accounts for the local wind forcing, while the latter represents wind forcing from remote regions outside the area of interest. Scale analysis which, for brevity, are not presented here suggests that insofar as barotropic responses are concerned, local forcing can be neglected if the domain size is far less than the Rossby radius (R), a condition certainly met by the present application. However, local wind forcing also generates surface-intensified current which significantly influences the near-field plume dispersal. For this reason, local wind forcing is retained to preserve accuracy.

4. NUMERICAL RESULTS

Figure 2 shows four surface circulation patterns after two days of easterly, westerly, northerly and southerly winds, serving as reference solutions before other forcings are introduced. Easterly and westerly winds drive strong windward coastal jets (in the order of 30-40 cm/s) over the shelf; Ekman veering is barely visible. By comparison, northerly and southerly winds generate much weaker windward currents (in the order of 10 cm/s), and even less Ekman veering. There are certain asymmetries between responses driven by easterly and westerly winds and between currents forced by northerly and southerly winds. A number of mechanisms could lead to the asymmetries. Alongshore topographic irregularity, the earth's rotation, the nonlinearity and any combination of these three is chiefly responsible. However, these asymmetries are too minor to be of major concern here. The conspicuous lack of the Ekman drift in these wind-driven responses is mainly caused by the proximity of the shoreline and is commented upon in the next section.



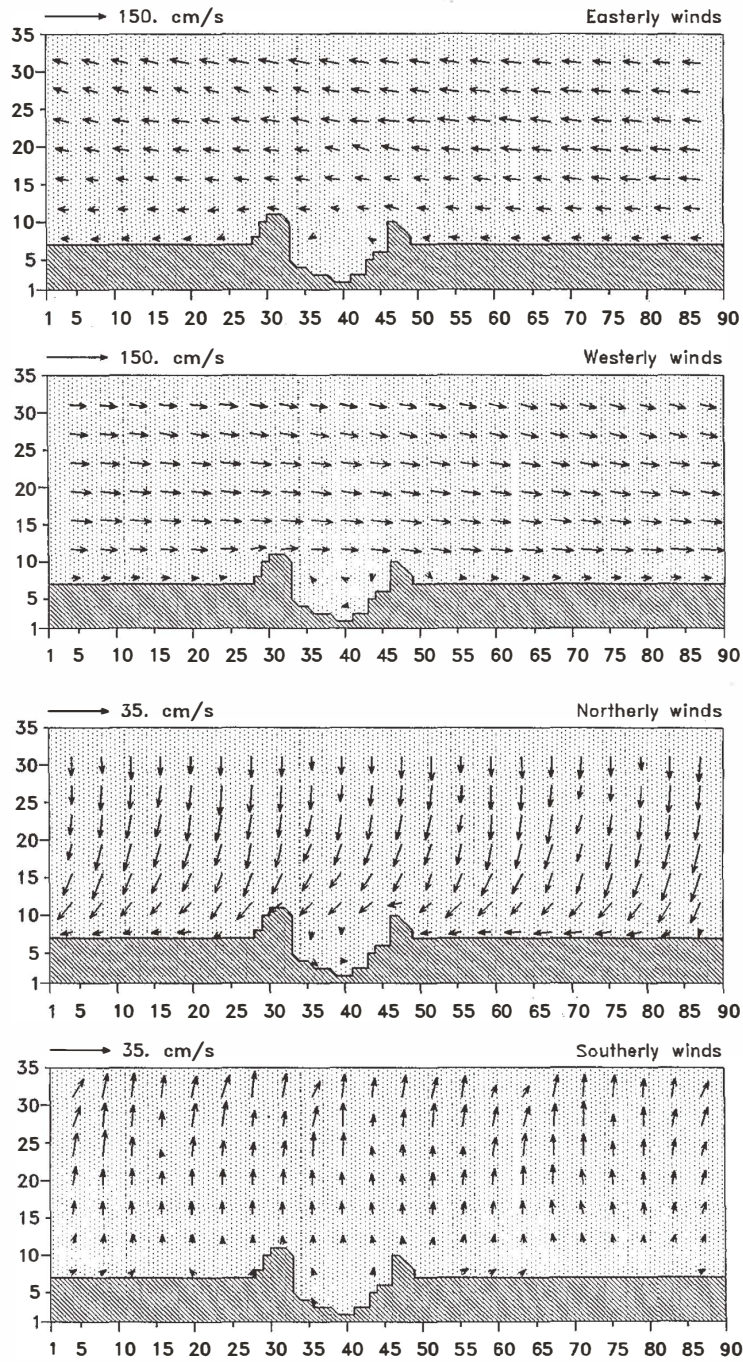
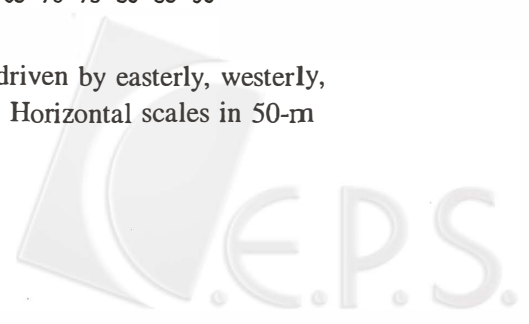


Fig. 2. Surface currents, from top to bottom panels, driven by easterly, westerly, northerly and southerly winds for two days. Horizontal scales in 50-m units.



Tide-plume interaction provides another reference point before the three-way interaction is discussed. This issue was extensively covered earlier by Lin *et al.* (1994). The major difference here is that tides enter the model through open boundary forcing rather than tidal generating force. In spite of the change, the plume responds to tides in a qualitatively similar manner to that in the early model. Figure 3 shows surface salinity and flow fields during the first tidal cycle of the third day after the plume release. The plume over the shelf oscillates in concert with the flood (westward) and ebb (eastward) currents but preferably hugs the coast during the ebb tide. This asymmetry was commented on earlier and is not restated here. Inside Yin-Yang Bay, the plume movement is out of phase with that over the shelf, apparently driven by recirculation eddies inside the embayment. More details can be found in Lin *et al.* (1994). In the absence of winds, the surface signature of plume water is rather expansive. This contrast is accentuated below.

The three-way interaction among wind-driven, tidally induced and river-forced motions is discussed below. Under easterly wind, Figure 4 shows surface salinity and flow fields during the first tidal cycle of the third day after the interaction is initiated. The easterly wind of 1 dyne/cm^2 generates a coastal jet which overpowers the tidal currents. The latter only weakly modulates the former. Inside the embayment, the plume water is confined to the windward half of the basin. Over the shelf, the downwind plume dispersal is concentrated nearshore. In this particular instance, periodic plume detachment over the shelf occurs preferably during the low slack water; with the timing, of course, depending on the strength of the wind forcing.

Figure 5 shows similar plume dispersal under the westerly wind during the first tidal cycle of the third day. The plume water inside the embayment is now restricted to the eastern half of the basin. Over the shelf, windward plume dispersal is also confined nearshore. Plume detachment under 1 dyne/cm^2 westerly wind occurs between high slack water and maximum ebbing, which releases fresher water eastward.

Under the northerly wind, plume expansion is compressed shoreward (Figure 6). Inside the bay, plume water follows its Kelvin wave instinct and concentrates on the eastern half of the basin most of the time, but not during low slack water when the plume is moved to the other side by the westward current. Over the shelf, the alongshore plume dispersal is in keeping with prevailing tidal currents: westward during flood period but eastward during ebb period.

Maximum flushing of the bay occurs under southerly wind, which unfortunately does not happen often in nature, partly because of the prevailing weather and partly due to the orographic blocking by the hills to the south. Under seaward wind, the plume disperses seaward with little lateral spreading (Figure 7). The lateral vibration of the plume trajectory is in keeping with tidal currents.

To better illustrate the effect of vertical mixing and in support of the argument below, Figure 8 shows the square of the Brunt-Vasaila frequency, the square of the vertical shear of the horizontal current, vertical eddy viscosity and diffusivity near the sea surface for the plume configuration corresponding to the upper-left panel of Figure 7. The ratio between the top-left and top-right gives the Richardson number. Regions of high Brunt-Vasaila frequency essentially overlap the plume. The vertical shear of the horizontal current is also the highest within the plume in the near-field, but it diminishes near the lateral plume boundaries. Interestingly, vertical viscosity and diffusivity are the highest along lateral plume boundaries in the near-field, where both the current shear and stability of the water column range from modest to low.



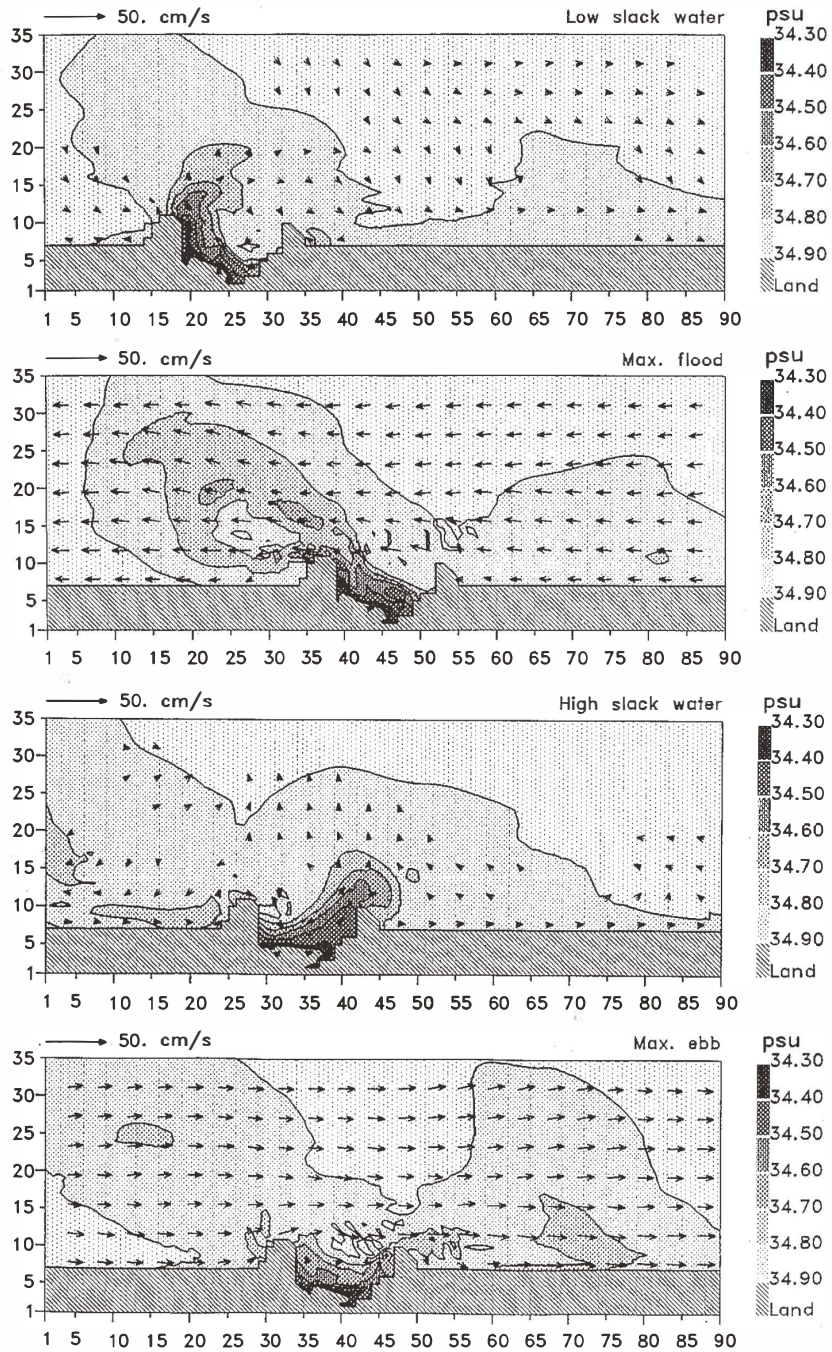


Fig. 3. Successive snapshots of surface flow and salinity fields during the first tidal cycle of the third day after plume release. There is no wind forcing. The contour interval for salinity is 0.1 psu, with the outermost contour of 34.9 psu separating the plume from ambient water. Horizontal scales in 50-m units.



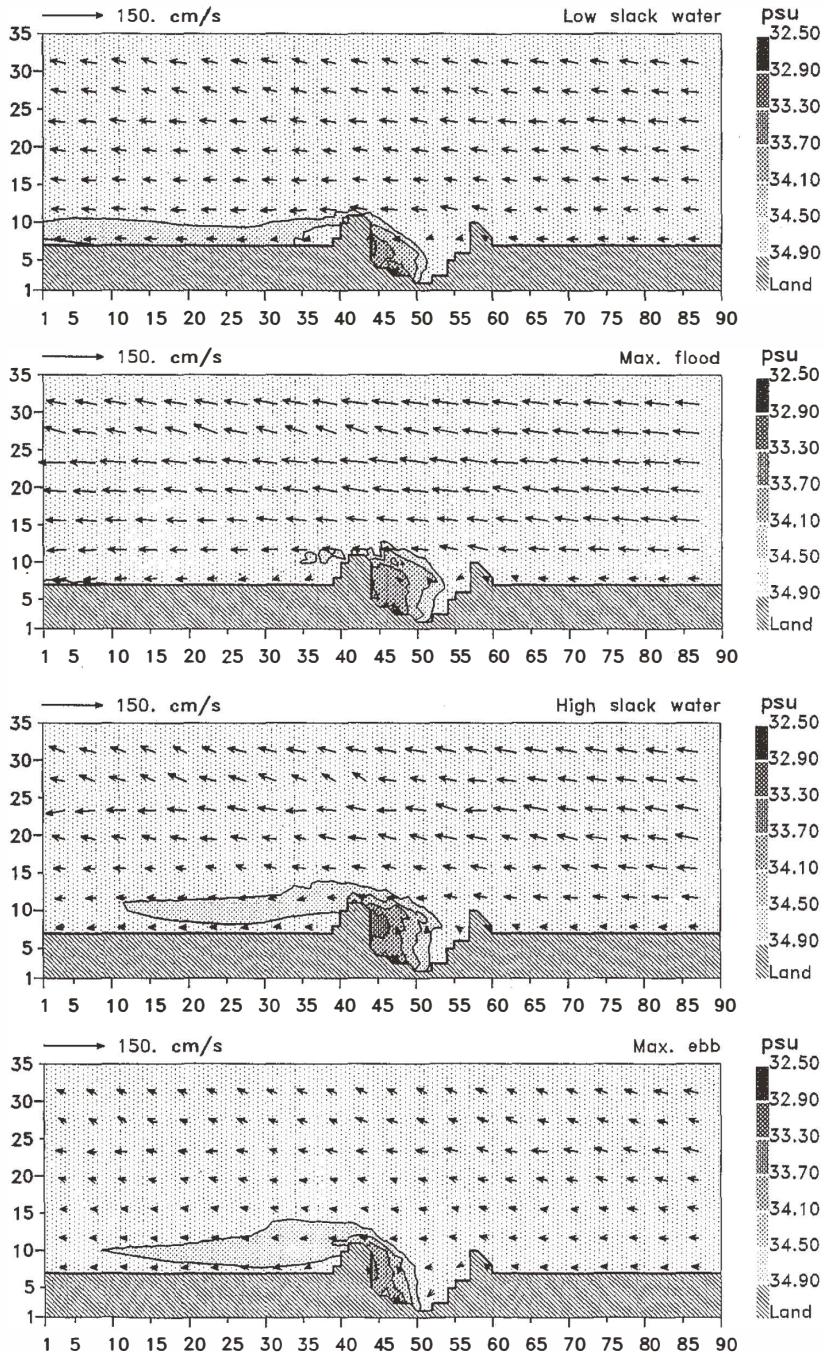


Fig. 4. Successive snapshots of surface flow and salinity fields during the first tidal cycle of the third day after the three-way (plume-tide-wind) interaction is initiated under easterly winds. The wind intensity is 1 dyne/cm^2 . Salinity contours are at intervals of 0.4 psu, with the outermost contour representing 34.9 psu. Horizontal scales in 50-m units.

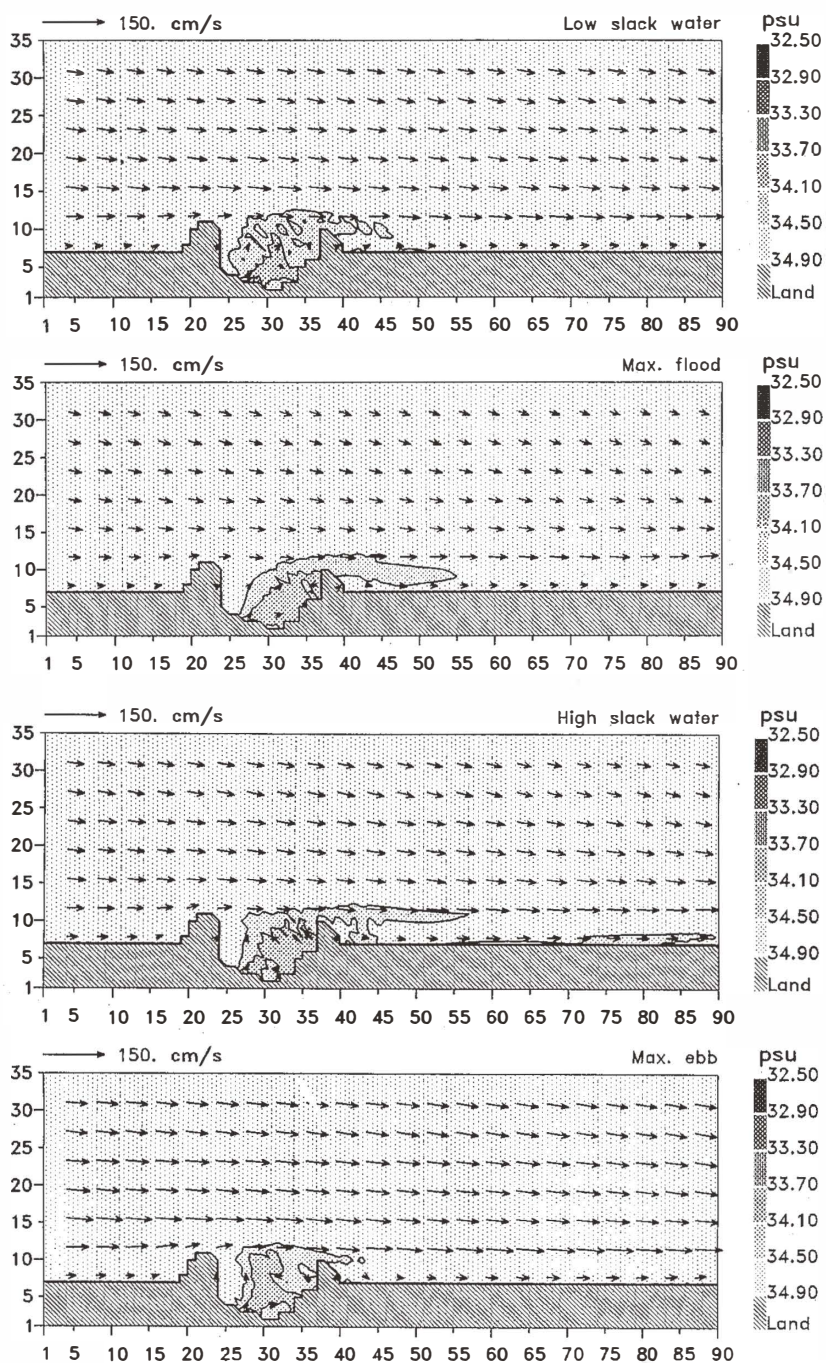


Fig. 5. As in Fig.4 except under westerly winds.



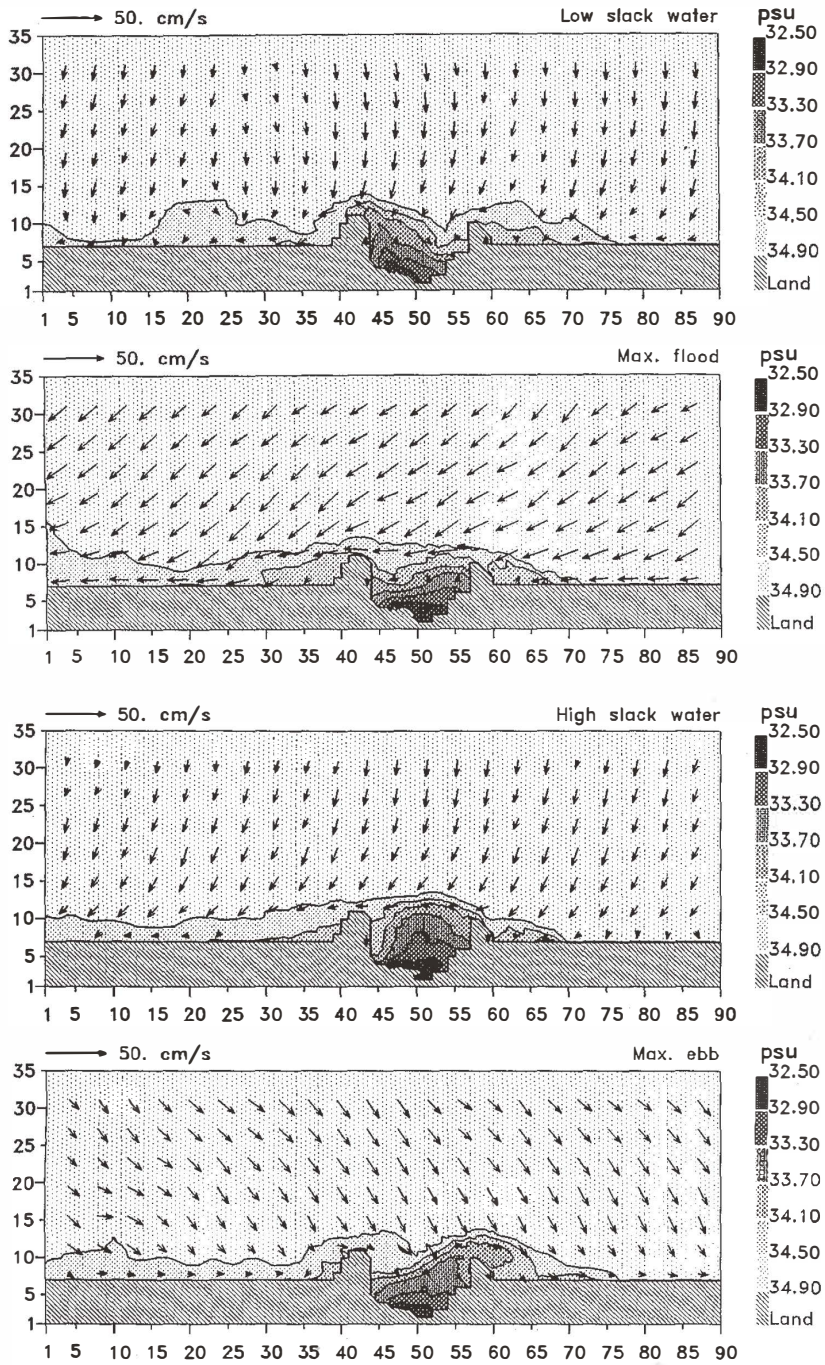


Fig. 6. As in Fig.4 except under northerly winds.



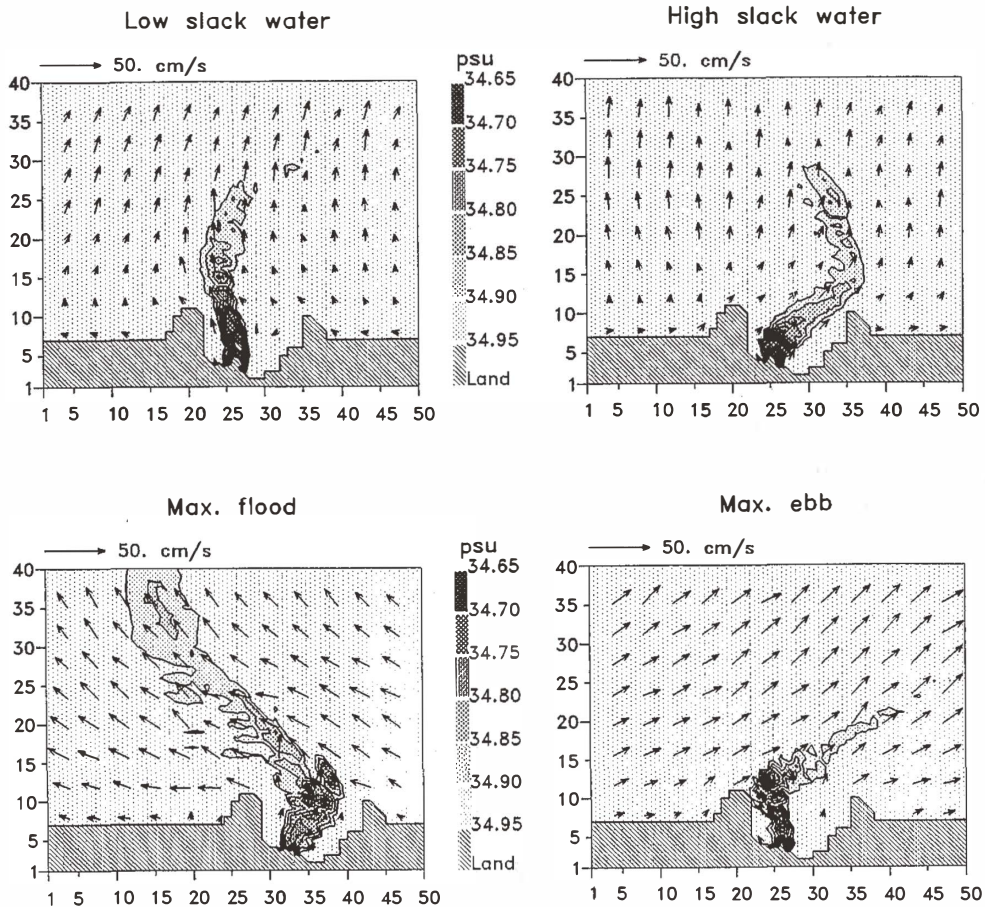


Fig. 7. Successive snapshots of surface flow and salinity fields during the first tidal cycle of the third day after the three-way interaction is initiated under southerly winds. Left: from low slack water to maximum flood. Right: from high slack water to maximum ebb. Salinity contours are at intervals of 0.05 psu with the outermost contour of 34.95 psu to better delineate the plume boundary. Horizontal scales and wind intensity are as same as in Fig.4.

With winds, the surface signature of the plume water is consistently less expansive. Part of the reason is due to the advection by wind-driven currents, because faster advection elongates a body of plume water. The other cause is the wind-enhanced vertical mixing in the mixed layer. Figure 8 shows that vertical diffusivity near the surface is consistently high along the lateral boundaries of the plume. In this model, vertical diffusivity is determined by the first-order closure scheme of Pacanowski and Philander (1981) although other schemes should also produce qualitatively similar behavior. The enhanced diffusivity mixes plume water downward along perimeters and narrows the surface plume in the process.

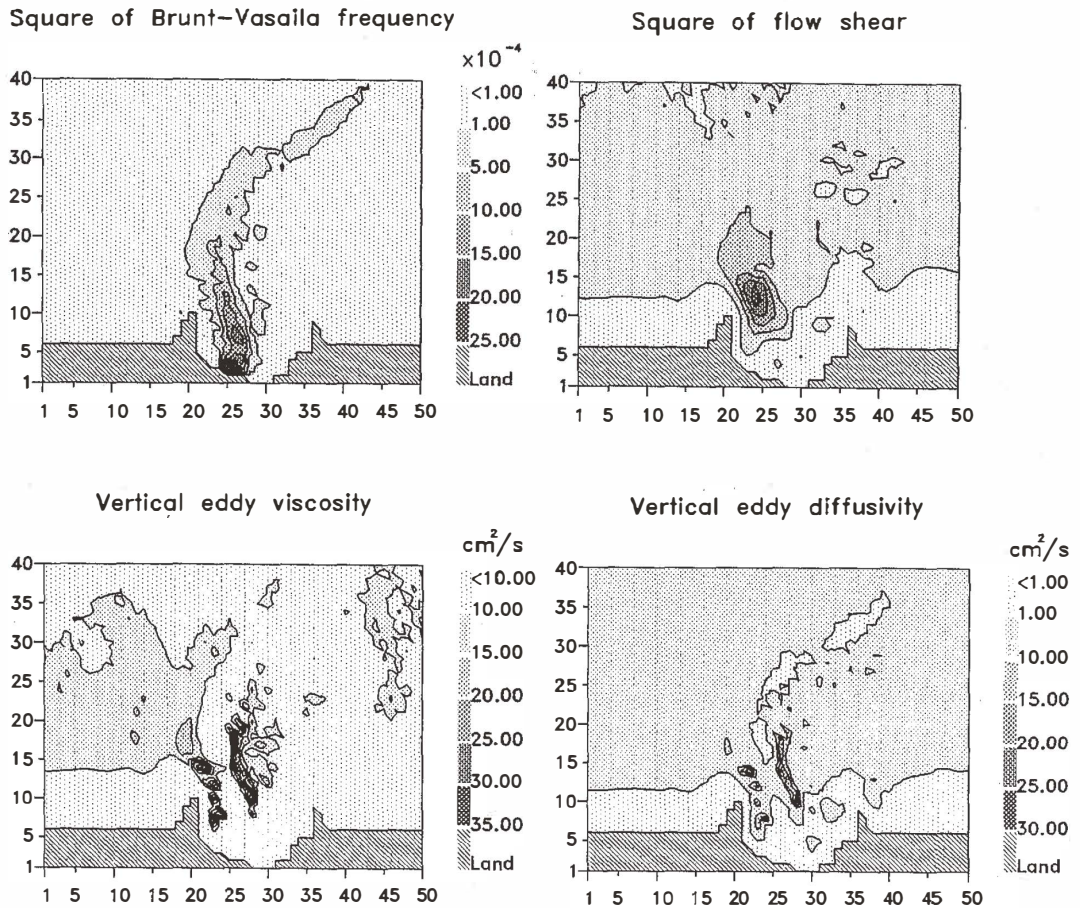


Fig. 8. The surface features of the square of the Brunt-Vasaila frequency, square of vertical shear of horizontal current, vertical eddy viscosity and diffusivity corresponding to the top-left panel of Fig. 7 (low slack water, southerly wind). Top two panels have the same calibration bars. Each bottom panel has its own calibration bar to the right. Horizontal scales in 50-m units.

It should also be emphasized that the plume dispersal under wind action is quite different from that of passive surface tracers. In general, river plumes differ from passive tracers in two ways. First, strong plumes may self-propagate as density currents, whereas tracers cannot. Second, plume water enhances stratification, reduces vertical viscosity and thereby hastens the wind-driven current near the surface. This interaction between plume-induced and wind-driven motions is also missing in the case of passive tracers. In the present application, the far-field plume distribution is much diluted; the first mechanism is therefore not important in the far field. The second mechanism is nevertheless strong enough to distinguish plume

water from passive tracers. To verify this, wind-driven solutions with and without the plume have been compared; windward surface current within the plume is consistently much higher than that outside the plume. Consequently, windward plume dispersal should be significantly faster than that of a passive tracer under identical forcing conditions.

5. DISCUSSION AND CONCLUSIONS

The three-way interaction among river-forced, wind-driven and tidally induced motions in the vicinity of Yin-Yang Bay is examined by analyzing a modest number of numerical simulations. The effort is not meant to be exhaustive, but rather to identify dominant physics governing the interaction, in light of the fact that the number of combinations among the strengths of these three forcings is countless. Insofar as the manner in which winds modulate a river plume is concerned, the picture emerging from this work deviates markedly from that derived from large-scale plume models. For large-scale plumes, the earth's rotational effect is far more important. In such cases, winds disperse river plumes primarily in the direction of the Ekman drift and windward dispersal is effective only under downwelling-favorable winds (Chao, 1988b). For small-scale plumes, the earth's rotating effect is somehow weakened. The consequent plume dispersal is mainly windward, except that a landward wind compresses plume water shoreward and subjects the eventual plume dispersal to tidal advection and density forcing. The mechanism leading to this discrepancy is discussed below.

Within several kilometers nearshore, wind-driven responses are significantly influenced by the pressure gradient force associated with sea level set-up or set-down. A seaward wind, for example, drives both an Ekman drift in response to the earth's rotation and a downwind current as a nonrotating response. The consequent coastal sea level set-down drives a geostrophic alongshore current opposing the Ekman drift and a nonrotating landward current, which also opposes the windward current. This renders the seaward wind ineffective in generating currents. The net result, as revealed by the present model, is essentially a weak seaward surface current. Conversely, a landward wind essentially produces a weak landward surface current.

An upwelling-favorable wind generates a seaward Ekman drift and a windward alongshore current as rotating and nonrotating responses, respectively. The consequent sea level set-down at the coast geostrophically induces an alongshore current reinforcing the wind-forced coastal jet, but also produces a down-pressure-gradient landward current opposing the Ekman drift. The net result is a much stronger windward coastal jet with little Ekman veering. Conversely, a downwelling-favorable wind also drives a strong windward coastal jet with little Ekman veering.

The foregoing rudimentary analysis points out the importance of sea level set-up or set-down within a coastal boundary layer several kilometers wide, inside which the consequent pressure gradient force always acts to offset the Ekman drift and keeps the wind-driven current windward. Further, it also explains why windward currents are much stronger under alongshore winds than under cross-shelf winds. Outside the coastal boundary layer, sea level set-up or set-down diminishes and the Ekman drift begins to dominate. In response to wind forcing, this makes large-scale plumes that spread farther out onto the shelf behave quite differently from small-scale plumes that are mainly confined nearshore. Large-scale plumes disperse in the direction of the Ekman drift; the maximum flushing of plume water is therefore achieved by upwelling-favorable winds. Small-scale plumes disperse windward, and offshore dispersal is most effective under seaward winds. The mechanism, as envisaged here, is quite

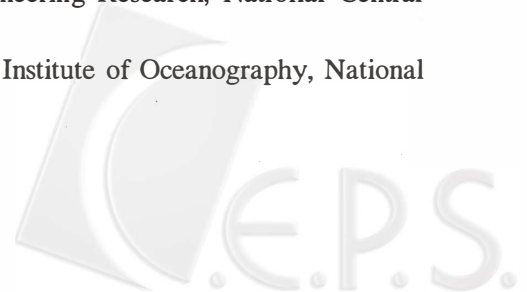
generic and one which is likely applicable to a wide range of small-scale plumes including the Yin-Yang plume.

In light of the model findings, it now seems feasible to plan management strategies about the Yin-Yang plumes as well as other river discharges based on the wind record alone. Before such cost-saving measures can be put into operation, however, a few comprehensive surveys of plume dispersals under different wind conditions will help put the practice on a solid footing.

Acknowledgments The research is supported by a grant from the National Science Council of the Republic of China under contract NSC-83-0209-M002A-024 and by the U.S. National Science Foundation under grant BSR-8814272 as part of the Land Margin Ecosystem Research.

REFERENCE

- Blumberg, A. F., and G. L. Mellor 1987: A description of a three-dimensional coastal ocean circulation model. In: N. S. Heaps (Ed.), *Three-dimensional Coastal Ocean Models*, Coastal and Estuarine Science, Vol. 4, Washington, DC: AGU, 1-16.
- Boicourt, W. C., S.-Y. Chao, H. W. Ducklow, P. M. Glibert, T. C. Malone, M. Roman, L. P. Sanford, J. Fuhrman, C. Garside, and R. Garvine 1987: Physics and Microbial ecology of a buoyant estuarine plume on the continental shelf. *EOS Trans. AGU*, **69**, 666-668.
- Chao, S.-Y. 1988a: River-forced estuarine plumes. *J. Phys. Oceanogr.*, **18**, 72-88.
- Chao, S.-Y. 1988b: Wind-driven motion of estuarine plumes. *J. Phys. Oceanogr.*, **18**, 1144-1166.
- Chao, S.-Y. 1990: Tidal modulation of estuarine plumes. *J. Phys. Oceanogr.*, **20**, 1115-1123.
- Chao, S.-Y., and W. C. Boicourt 1986: Onset of estuarine plumes. *J. Phys. Oceanogr.*, **16**, 2137-2149.
- Chao, S.-Y., and T. Paluszkiwicz 1991: The hydraulics of density currents over estuarine sills. *J. Geophys. Res.*, **96**, 7065-7076.
- Csanady, G. T. 1974: Barotropic currents over the continental shelf. *J. Geophys. Res.*, **4**, 357-371.
- Csanady, G. T. 1984: *Circulation in the Coastal Ocean*. D. Reidel Pub. Co., Dordrecht, Holland, 279pp..
- Garvine, R. W. 1974: Physical features of the Connecticut River outflow during high discharge. *J. Geophys. Res.*, **79**, 831-846.
- Li, C.-C., T.-H. Ts'ang, C.-H. Chang, C.-T. Chuang, L.-Y. T'sai, and K.-T. Kuo 1991: The formation study and preliminary environmental protection design of Yin-Yang Bay. Special Pub. No. 20, Center for Environmental Engineering Research, National Central University, 788pp. (in Chinese).
- Lien, S.-L. 1977: Tidal prediction model. Special Pub., Institute of Oceanography, National Taiwan University, 225pp. (in Chinese).



- Lin, C.-T., K.-L. Fan, and S.-Y. Chao 1994: Small-scale plumes from a semi-enclosed basin: Yin-Yang Bay. *TAO*, **5**, 91-107.
- Masse, A. K., and C. R. Murthy 1990: Observations of the Niagara River thermal plume (Lake Ontario, North America). *J. Geophys. Res.*, **95**, 16097-16109.
- O'Donnell, J. 1990: The formation and fate of a river plume: a numerical model. *J. Phys. Oceanogr.*, **20**, 551-568.
- Pacanowski, R. C., and S. G. H. Philander 1981: Parameterization of vertical mixing in numerical models of tropic oceans. *J. Phys. Oceanogr.*, **11**, 1443-1451.
- Semtner, A. J. 1974: An oceanic general circulation model with bottom topography. Numerical Simulation of Weather and Climate, Tech. Rep. 9, Dept. of Meteorology, UCLA, 99pp.
- Shaw, P.-T., and S.-Y. Chao 1994: Surface circulation in the South China Sea. *Deep Sea Res.*, **41**, 1663-1683.
- Stumpf, R. P., G. Gelfenbaum, and J. R. Pennock 1993: Wind and tidal forcing of a buoyant plume, Mobile Bay, Alabama. *Contin. Shelf Res.*, **13**, 1281-1301.

